ARTICLE NO. 79-1784R

G 80 - 074

00016
00017

Structural Model of the Adaptive Human Pilot

Ronald A. Hess*
NASA Ames Research Center, Moffett Field, Calif.

A compensatory tracking model of the human pilot is offered, which attempts to provide a more realistic representation of the human's signal processing structure than that which is exhibited by pilot models currently in use. Two features of the model distinguish it from other representations of the human pilot. First, proprioceptive information from the control stick or manipulator constitutes one of the major feedback paths in the model, providing feedback of vehicle output rate due to control activity. Implicit in this feedback loop is a model of the vehicle dynamics which is valid in and beyond the region of crossover. Second, error rate information is continuously derived and independently but intermittently controlled. An output-injected remnant model is offered and qualitatively justified on the basis of providing a measure of the effect of inaccuracies such as time variations in the pilot's internal model of the controlled-element dynamics. The data from experimental tracking tasks involving five different controlled-element dynamics and one nonideal viewing condition were matched with model-generated describing functions and remnant power spectral densities.

Nomenclature

$C_x(j\omega_k)$ = Fourier coefficient of $x(t)$ at frequency ω_k
d = disturbance
e = system error
e_d = displayed error
$E[A]$ = expected value of A
$F_x(j\omega,P_1)$ = spectral measure of $x(t)$ with switching probability of P_1
$[F_x(j\omega)]'$ = $(1-P_1)\cdot F_x(j\omega,0)+P_1\cdot F_x(j\omega,1)$
j = imaginary unit
k = order of Y_c in region of crossover
K = controlled-element gain
$K_e,K_{\dot{e}},K_1,K_2$ = pilot model gains
m = system output
n_{e_d} = pilot displayed error-injected remnant
n_u = pilot output-injected remnant
P_1 = probability of model switch being in position 1
s = Laplace variable
T_1,T_2 = pilot model time constants
u_δ = pilot output
Y_c = controlled-element dynamics
Y_{d_e} = display dynamics
$|A/B|$ = absolute value of ratio of complex numbers A and B
$\angle A/B$ = phase angle of ratio of complex numbers A and B
ζ_n = damping ratio of open-loop neuromuscular system
ρ = remnant scale factor
σ_x = root mean square (rms) value of variable $x(t)$

$$= \left[\lim \frac{1}{2T}\int_{-T}^{T} x^2(t)\,dt\right]^{1/2},$$

$$\left[\frac{1}{2}\int_{-\infty}^{\infty} \Phi_{xx}(\omega)\,d\omega\right]^{1/2}$$

τ_0,τ_1 = pilot model time delays
Φ_{xx_a} = power spectral density of variable x_a
ω = frequency
ω_n = undamped natural frequency of neuromuscular system

Received June 11, 1979; presented as Paper 79-1784 at the AIAA Guidance and Control Conference, Boulder, Colo., Aug. 6-8, 1979; revision received Nov. 26, 1979. This paper is declared a work of the U.S. Government and therefore is in the public domain.
Index categories: Guidance and Control; Handling Qualities, Stability and Control.

*Research Scientist. Member AIAA.

Introduction

ANALYTICAL techniques for pilot modeling tend to fall into two categories, a dichotomy shared with control system design techniques in general. These are the so-called "classical" and "modern" approaches. The classical approach has led to the development of the "servo model" of the human pilot.[1] In this model, a servolike operation on a single stimulus (system error) by the pilot is hypothesized. The modern approach has yielded the "optimal control model" of the human pilot[2] in which the pilot's dynamic characteristics are likened to those of an optimal state estimator and regulator, and the pilot is assumed to operate on a vector stimulus of error and error rate. Both of these models have their particular merits and practitioners and both have been applied to similar analysis/design problems with reasonable success. These applications range from describing pilot dynamics in single-axis tracking tasks[1,2] to cockpit display design,[3,4] to handling qualities investigations,[5,6] and to motion cue research.[7,8]

Despite their relative successes, neither the servo model nor the optimal control model attempts to describe the underlying structure which contributes to human pilot dynamics. Rather, these models have evolved as expedient means for quantifying the general transfer and performance characteristics of the human pilot in specific tracking tasks. Following the lead of Smith,[9] Hess[10] has attempted to provide a more satisfactory structural model of the human pilot. The impetus behind the research of Refs. 9 and 10 and that reported here is the conviction that a pilot model, which provides a more realistic representation of the signal processing structure of the human pilot, will also provide a more unified theoretical framework within which to interpret a variety of empirical pilot/vehicle response phenomena. The particular phenomena to be discussed here will include the ability of the pilot to adapt to different vehicle dynamics and to displays of varying quality. As used here, "adaption" refers to the ability of the pilot to change his dynamic characteristics, through training, to suit the task at hand.

Model Specifics

The model which is the subject of this paper is an outgrowth of the research described in Refs. 9-11. A block diagram

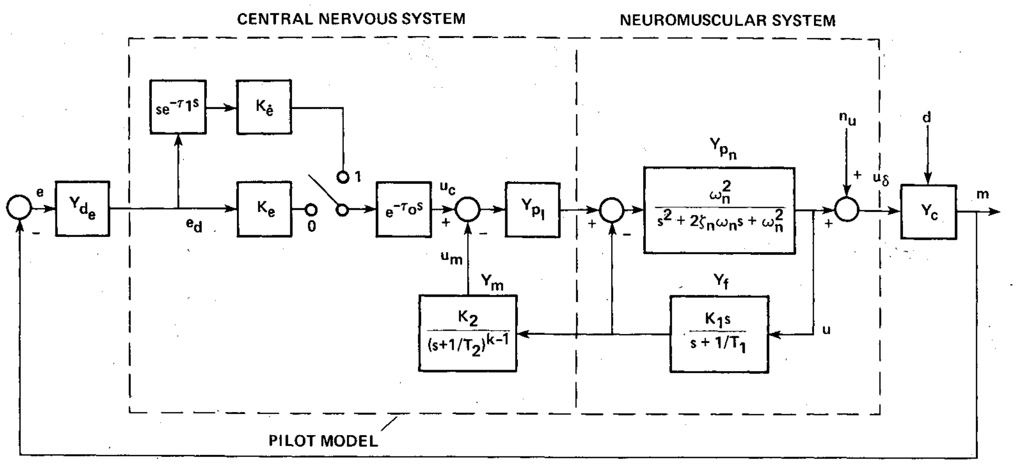

Fig. 1 Structural model of the adaptive human pilot.

representation of the model, suitable for describing such single-axis pilot behavior as pitch attitude tracking in the presence of atmospheric turbulence, is shown in Fig. 1.

The model has been divided into central nervous system and neuromuscular system components, a division which is intended to emphasize the nature of the signal processing activity involved. System error $e(t)$ is presented to the pilot via a display with dynamics Y_{d_e}. The rate of change of the displayed error is assumed to be derived from $e_d(t)$. The process of deriving error rate is assumed to entail a computational time delay of τ_1 seconds. Constant gains K_e and $K_{\dot{e}}$ multiply the signals $e_d(t)$ and $\dot{e}_d(t-\tau_1)$, respectively. The switch allows either of these two signals to be used as driving signals to the remainder of the model. In this study, the action of the switch will be parameterized by the variable P_1, which represents the probability that the switch will be in position 1 (error-rate control) at any instant of time. A central time delay of τ_0 seconds is included to account for the effects of latencies in the visual (aural or tactile) process sensing $e_d(t)$, motor nerve conduction times, etc. The resulting signal $u_c(t)$ provides a command to a closed-loop system consisting of "pulsing logic" Y_{P_1}, a model of the open-loop neuromuscular dynamics of the particular limb driving the manipulator Y_{p_n}, and elements Y_f and Y_m which emulate, at least approximately, the combined effects of the muscle spindles and the dynamics associated with higher-level signal processing. A colored noise $n_u(t)$ is injected at the pilot's output as remnant.

Let us look at each of the model elements now in a bit more detail. The assumption that error rate is a derived rather than a sensed quantity is conservative in nature. In terms of visual stimuli, arguments still abound as to whether motion in the visual field of the human is perceived "directly" as a primary psychological attribute of the visual system, or whether it is inferred or is a calculated or secondary attribute based on memory for position.[12] In terms of the model, the question of direct vs derived rate inputs will influence the magnitude of the time delay τ_1, i.e., for direct rate perception τ_1 will be negligible, whereas for derived rate inputs, a significant τ_1 may be indicated. Since, here, the stimulus $e_d(t)$ can be visual, aural, or tactile, it was assumed that $\dot{e}_d(t)$ was a derived quantity. A simple model for such rate derivation was offered by McRuer et al.[13] in the form of a "differential-displacement" model. As a conservative estimate of the sampling delay occurring in such a model, let us use $\tau_1 = 0.2$ s. The time delay τ_0 can be broken down into constituent components, at least in approximate fashion. For visual stimuli, which will constitute the modality for the data to be utilized later, we have the following average values[13]:

Latency of the visual process, s	0.075
Motor nerve conduction time, s	0.030
Central processing time, s	0.030
	0.135

The value $\tau_0 = 0.14$ s was used here.

A discussion of appropriate pulsing logic was carried out previously by Hess[11] and will not be dealt with here. This logic is used to generate the pulsive control behavior evident when the pilot is faced with higher order-controlled element dynamics such as K/s^2 or K/s^3. In this study, $Y_{P_1} = 1.0$. The form of the open-loop neuromuscular dynamics Y_{P_n} is based upon electromyogram measurements reported in Ref. 14. The following values of ω_n and ζ_n were selected based upon that work:

$$\omega_n = 10 \text{ rad/s} \quad \text{and} \quad \zeta_n = 0.707$$

The feedback loop in Fig. 1 involving Y_f alone is intended to represent, in approximate fashion, the feedback activity of the muscle spindles in the limb driving the manipulator or control stick. For the purposes of this study, $K_1 = 1.0$. The washout characteristics of the element Y_f are important to the overall model dynamic characteristics, as will be seen. The physiological source of such a washout, if it indeed exists, is unknown. Its existence is part of the basic structural hypothesis of the model. From a functional standpoint, the muscle spindle is a length transducer transforming increases in extrafusal muscle fiber length from some set or operating point into electrical impulses. Anatomically, the spindles are in parallel with the extrafusal fibers. One possibility is that the washout characteristics are a consequence of the intrafusal fibers of the spindle tracking the low-frequency changes in the length of extrafusal fibers in the agonist-antagonist muscle pairs in the limb driving the manipulator. A necessary condition for such coactivation of muscle fibers would be concomitant coactivation of the motor fibers which innervate the extra- and intrafusal fibers, respectively. Such a coactivation has been documented by physiologists and given the name "alpha-gamma linkage."[15]

The form of the element Y_m is assumed to depend on the order of a simplified model of the controlled-element dynamics valid in the frequency range where $Y_p \cdot Y_c \doteq 1.0$, i.e., open-loop crossover. For all but two of the controlled elements to be studied here, no simplification is necessary. In general, $\hat{Y}_c(s) \doteq Ks^k$, $k = 0, \pm 1, \pm 2, \ldots$, etc., where $\hat{Y}_c$ is an approximation to Y_c valid in the region of open-loop crossover.[10,11] Note that manipulator dynamic characteristics can be lumped into Y_c. Evidence supporting the hypothesis of a proprioceptive-related internal model has recently been offered by Kessel and Wickens.[16] The use of the factor $(s+1/T_2)^k$ in Y_m ($T_2 \doteq T_1$) rather than simply s^k was found to be necessary to achieve acceptable describing function matches with experimental data. The inclusion of this term is tantamount to saying that no low-frequency processing of spindle output takes place in the higher levels of the nervous system, only spindle output itself is utilized, attenuated, or magnified by an appropriate gain K_2. For the sake of simplicity, $T_2 = T_1$ in all that follows. Note that in the region of open-loop crossover, the signal $u_m(t)$ is an estimate of the rate of change of the controlled-element output due to control activity $u_\delta(t)$, excluding the contributions due to disturbance $d(t)$ and remnant $n_u(t)$. Thus, this loop is a form of rate feedback in the model.

The physical interpretation of remnant depends on the particular pilot model with which it is associated. The servo model had its origins in nonlinear describing function theory, and remnant for that model tends to be thought of, indeed defined, as that portion of the pilot's output not linearly correlated with the disturbance. The tacit interpretation here is that remnant arises from nonlinearities and/or time variations in the human pilot. In the optimal control model, which obviously had its origins in linear optimal estimation and control theory, remnant tends to be viewed in terms of "observation noise." Here the interpretation is that all observations which the pilot makes are corrupted by white noise. This is not to say that there is no underlying equivalence in these views,[17] but rather that the physical interpretation of remnant is often determined by the genesis of the pilot model itself. This is as it should be. In the model of Fig. 1, the pilot's internal representation of the controlled-element dynamics is hypothesized to form a pivotal part of the equalization capability of the pilot. Thus, inaccuracies, such as time variations, in this internal model representation can be logically considered a primary source of remnant. Furthermore, this remnant should be amenable to representation as a "process noise" in that it is intended to account, in stochastic fashion, for the effects of imprecise internal model parameterization,[18] whatever the source of this imprecision. Thus, in Fig. 1, the remnant $n_u(t)$ is shown injected into the pilot's output and, as such, acts as a true process noise in terms of the vehicle to be controlled.

With this discussion in mind, two hypotheses will be made regarding the nature of this injected noise. The first hypothesis asserts that the variance of $n_u(t)$ scales with the variance of the system error normalized by the manipulator/controlled element static gain. This means the variance of the noise scales with $\sigma^2_{e_d}/K^2\,|Y_{d_e}(j\omega)|^2$, where $\sigma^2_{e_d}$ is the variance of the displayed error, $Y_{d_e}(j\omega)$ is the display dynamics (typically a gain), and K is the manipulator/controlled element static gain. The second hypothesis asserts that the process noise power is attenuated at frequencies beyond the bandwidth of the human pilot. This limitation can most easily be accommodated in the model by considering $n_u(t)$ to be a colored noise with a bandwidth determined by the position of the closed-loop neuromuscular mode roots of the describing function portion of the pilot model.

The idea that the variance of $n_u(t)$ should scale with normalized system error means that $n_u(t)$ is not multiplicative noise in that it does not scale with the variance of the signal to which it is added. The first hypothesis is based on the reasonable supposition that gain-normalized system-error variance is a sensitive indicator of errors in the pilot's internal representation of the controlled-element dynamics. The assertion that the control-injected remnant variance scales linearly with this error variance is an assumption to be verified on the basis of experiment. The second hypothesis seems almost self-evident; there can be no significant effects attributable to internal model errors at frequencies well beyond the bandwidth of the structure which contains the internal model, i.e., the pilot.

The model for the power spectral density of the injected remnant $n_u(t)$ can now be given as

$$\Phi nn_u(\omega) = \rho\cdot\frac{\sigma^2_{e_d}}{K^2\,|Y_{d_e}(j\omega)|^2}\;\frac{(1/T_3)^2}{[\omega^2+(1/T_3)^2]}$$

where ρ is a scale factor to be empirically determined and $1/T_3$ represents the undamped natural frequency of the closed-loop neuromuscular mode roots of the describing function portion of the pilot model. On the basis of remnant data for pure gain controlled-element dynamics, a value of $\rho=0.38$ was selected via the data fitting procedure to be described. This value was then used in the remnant model for all of the controlled-element dynamics studied herein.

By referring to Fig. 1, one can see that, with the switch in position 1, the time delay for error rate tracking is $\tau_0+\tau_1=0.34$ s. The magnitude of this delay will obviously result in a compromise between responsiveness and stability for the rate tracking loop. Since error rather than error rate tracking will predominate in the model, it was felt that the responsiveness of the error rate loop should take precedence over relative stability characteristics. Therefore, in the data fitting to be described, the gain $K_{\dot e}$ will be made as large as possible under the single constraint of guaranteeing only absolute stability in the rate tracking loop.

Data Fitting

As employed here, the model of Fig. 1 will be a data summary rather than a predictive model of the human pilot. We will not attempt to make predictions about the behavior of the pilot/vehicle system under situations which have not been previously tested. Here data are intended to mean the frequency domain measures of describing function and remnant power spectral density. In the available experimental data to be utilized in the fitting or matching procedure, the pilot model remnant was assumed to be injected at the pilot's input rather than his output. Therefore, in order to compare the experimental and model remnant spectra, we will use the output-injected remnant model just discussed to obtain equivalent input-injected (error) spectra. Let us now turn our attention to such a data matching procedure.

The following parameters will be at our disposal in varying the frequency domain characteristics of the structure of Fig. 1: the gains K_e, $K_{\dot e}$, and K_2; the time constant T_1; and the error rate control probability P_1. The remaining variables: k, K_1, T_2, T_3, ζ_n, ω_n, τ_0, τ_1, and ρ will either be obvious from the task (i.e., k is determined once Y_c is specified) or be functions of the former five variables, e.g., $T_2=T_1$, $T_3=f(\zeta_n,\omega_n,K_2,T_1)$, or simply be held fixed at empirically determined values. The decision of which variables to vary and which to hold fixed is not entirely arbitrary. The variables τ_0, τ_1, ζ_n, ω_n, K_1, and, to some extent, ρ are intended to be strongly isomorphic with the physiology of the human pilot, at least at the level of detail possible in the structure of Fig. 1. While it is not difficult to imagine rather small intertask variations in these parameters, large variations are somewhat less palatable, at least to this author. Said another way, one should not be forced to consistently hypothesize 25-50% variations in basic (as opposed to "effective") time delays or open-loop neuromuscular parameters in order to interpret pilot-response phenomena. On the other hand, the variables K_e, $K_{\dot e}$, K_2, P_1, and, to some extent, T_1 represent the central processing part of the structure of Fig. 1. Large variations in these parameters from task to task are certainly not unreasonable.

Were it not for the existence of the switch in Fig. 1, calculating model describing functions and remnant spectra would be a simple exercise in block diagram algebra. The switch and its operation form an important part of the model, however, and represent a significant departure from the model of Refs. 10 and 11. Given the model with some fixed set of parameters, the question to be answered is: What describing function $Y_p(j\omega)$ and error-injected remnant power spectral density $\Phi_{nn_e}(\omega)$ would be obtained by making spectral measurements of $u_\delta(t)$ and $e_d(t)$ over some fixed run length with the switch randomly moving between positions 0 and 1 and with the probability of being at position 1 of P_1? To answer this question, one could, of course, simulate the model and actually make the measurements using typical spectral techniques such as the fast Fourier transform. However, this would be computationally quite expensive, particularly since many such runs would be required to select the proper model parameters to fit the data. Consider, instead, the following approximate development. Let $u_\delta(t)$ and $e_d(t)$ represent the time histories of model input and output in a single run with the switch operating as just described. Concentrating on $u_\delta(t)$, let $F_{u_\delta}(j\omega,P_I)$ represent a spectral measure (Fourier coefficient or power spectral density) of $u_\delta(t)$. Expanding $F_{u_\delta}(j\omega,P_I)$ in a Taylor series about the point $P_I=0$,

$$F_{u_\delta}(j\omega,P_I)=F_{u_\delta}(j\omega,0)+\left.\frac{\partial F_{u_\delta}(j\omega,P_I)}{\partial P_I}\right|_{P_I=0}P_I+\frac{1}{2!}\left.\frac{\partial^2 F_{u_\delta}(j\omega,P_I)}{\partial P_I^2}\right|_{P_I=0}P_I^2+\text{higher order terms}$$

Now, since $P_I<1$ (for the cases to be studied here, $P_I\leq 0.25$), we can write

$$F_{u_\delta}(j\omega,P_I)\doteq F_{u_\delta}(j\omega,0)+\left.\frac{\partial F_{u_\delta}(j\omega,P_I)}{\partial P_I}\right|_{P_I=0}P_I$$

Further, let us approximate

$$\left.\frac{\partial F_{u_\delta}(j\omega,P_I)}{\partial P_I}\right|_{P_I=0}\doteq\frac{F_{u_\delta}(j\omega,1)-F_{u_\delta}(j\omega,0)}{(1-0)}$$

Therefore, we can state

$$F_{u_\delta}(j\omega,P_I)\doteq(1-P_I)F_{u_\delta}(j\omega,0)+P_IF_{u_\delta}(j\omega,1)$$

For efficiency, let us denote the right-hand side of the above equation as $[F_{u_\delta}(j\omega)]'$, dropping the P_I notation for convenience. Thus, we have

$$F_{u_\delta}(j\omega)\doteq[F_{u_\delta}(j\omega)]'=(1-P_I)F_{u_\delta}(j\omega,0)+P_IF_{u_\delta}(j\omega,1)$$

A similar relation can, of course, be obtained for $F_{e_d}(j\omega)$.

Reference 19 offers a simple but quantitative example of the quality of this approximation procedure and also indicates that, in terms of frequency domain measures, the switching operation can be successfully parameterized by the single quantity P_I. Measured Fourier coefficients appear to be relatively insensitive to the minimum duration of switch closure for a range of values (0.5-5.0 s) deemed appropriate for the tracking tasks to be utilized here.

Now with a sum of sinusoids disturbance, the model describing function $Y_p(j\omega_k)$, which would be measured in the single run with the switch operating randomly, can be approximated as

$$Y_p(j\omega_k)=\frac{C_{u_\delta}(j\omega_k)}{C_{e_d}(j\omega_k)}\doteq\frac{[C_{u_\delta}(j\omega_k)]'}{[C_{e_d}(j\omega_k)]'}\tag{1}$$

With remnant $n_{e_d}(t)$ injected at the displayed error $e_d(t)$, we have, for the power spectral density of the model output at frequencies ω_j,

$$\Phi uu_\delta(\omega_j)=|C_{u_\delta}(j\omega_j)|^2=\frac{\Phi_{nn_{e_d}}(\omega_j)\left|\dfrac{C_{u_\delta}(j\omega_j)}{C_{e_d}(j\omega_j)}\right|^2}{\left|1+\dfrac{C_{u_\delta}(j\omega_j)}{C_{e_d}(j\omega_j)}\cdot Y_c(j\omega_j)\right|^2}\tag{2}$$

where the ω_j occur between disturbance frequencies ω_k and $C_{u_\delta}(j\omega_j)$ and $C_{e_d}(j\omega_j)$ are obtained by averaging their values at the disturbance frequencies to either side of ω_j. With remnant $n_u(t)$ injected at the model output, we can write

$$[\Phi uu_\delta(\omega j)]'=[|C_{u_\delta}(j\omega_j)|^2]'=\left[\frac{\Phi_{nn_u}(\omega_j)}{\left|1+\dfrac{C_{u_\delta}(j\omega_j)}{C_{e_d}(j\omega_j)}\cdot Y_c(j\omega_j)\right|^2}\right]'\tag{3}$$

Again, the measured power spectral density of the model output $u_\delta(t)$ with the switch in operation can be approximated as

$$\Phi_{uu_\delta}(\omega_j)\doteq[\Phi_{uu_\delta}(\omega_j)]'\tag{4}$$

Thus,

$$\Phi_{nn_{e_d}}(\omega_j)\doteq\left[\frac{\Phi_{nn_u}(\omega_j)}{\left|1+\dfrac{C_{u_\delta}(j\omega_j)}{C_{e_d}(j\omega_j)}\cdot Y_c(j\omega_j)\right|^2}\right]'\cdot\frac{|1+Y_p(j\omega_j)Y_c(j\omega_j)|^2}{|Y_p(j\omega_j)|^2}\tag{5}$$

Equations (1) and (5) will allow us to approximate the model describing functions and error-injected remnant power spectral densities which would be "measured" in a single run with the switch in operation by spectral measures obtained with the switch either in the 0 or 1 position for the entire run.

Finally, in order to avoid the necessity of actually making simulation runs to obtain the spectral measures, the complex number on the right-hand side of Eq. (1) will be expressed in magnitude and phase form as

$$|Y_p(j\omega_k)|=\left|\frac{[C_{u_\delta}(j\omega_k)]'}{[C_{e_d}(j\omega_k)]'}\right|\doteq\log^{-1}\left\{\left[\log\left|\frac{C_{u_\delta}(j\omega_k)}{C_{e_d}(j\omega_k)}\right|\right]'\right\}\tag{6}$$

$$\angle Y_p(j\omega_k)=\angle\frac{[C_{u_\delta}(j\omega_k)]'}{[C_{e_d}(j\omega_k)]'}\doteq\left[\angle\frac{C_{u_\delta}(j\omega_k)}{C_{e_d}(j\omega_k)}\right]'\tag{7}$$

where $C_{u_\delta}(j\omega_k)/C_{e_d}(j\omega_k)$ is now merely the algebraically obtained expression for the model transfer function with the switch in either the 0 or 1 position. Equations (6) and (7) thus allow simple algebraic averages in the frequency domain to replace Fourier transformations in the time domain. The accuracy of the relations on the right-hand side of Eqs. (6) and (7) was appraised by creating two sets of complex numbers A and B, whose real and imaginary parts were randomly selected from a population with a Gaussian distribution possessing a mean of 0.5 and a standard deviation of unity. Each set contained 5000 complex numbers. The primed operations on the middle and right-hand sides of Eqs. (6) and (7) were generalized by considering the expected values of A and B (denoted by $E[A]$, $E[B]$, respectively). Values for $|E[A]/E[B]|$ and $\angle E[A]/E[B]$ corresponding to an arbitrarily large sample size would be 1.0 and 0 deg, respectively. The actual values generated for a sample size of 5000 were

$$|E[A]/E[B]|=1.009\quad \log^{-1}\{E[\log|A/B|]\}=1.01$$

$$\angle E[A]/E[B]=-1\text{ deg}\quad E[\angle A/B]=1.75\text{ deg}$$

Table 1 Pilot model parameter values used to generate describing functions and remnant power spectral densities in Figs. 2-7

Controlled-element dynamics	Model parameters											
	k	K_e	$K_{\dot{e}}$	K_2	P_I	T_I	K_I	τ_0	τ_I	ζ_n	ω_n	ρ
K	0	11.1	2.13	2.0	0.05	5.0	1.0	0.14	0.2	0.707	10.0	0.38
K/s	1	22.2	3.42	2.0	0.05	5.0	1.0	0.14	0.2	0.707	10.0	0.38
K/s^2	2	26.2	10.50	10.0	0.20	2.5	1.0	0.14	0.2	0.707	10.0	0.38
$K/s(s-1)$	2	89.6	28.6	30.0	0.20	1.0	1.0	0.14	0.2	0.707	10.0	0.38
$K/s(s^2+1.414s+1)$	3	116.0	13.0	35.0	0.20	0.85	1.0	0.14	0.2	0.707	10.0	0.38
$K/s\|_{\text{peripheral}}$	1	12.6	2.52	0.75	0.25	5.0	1.0	0.14	0.2	0.707	10.0	0.38

The expressions on the right-hand sides of Eqs. (6) and (7) are seen to provide very satisfactory approximations for our purposes.

The validity of the approximate analysis just described obviously depends upon the validity of Eqs. (1) and (4) and the relations which preceded them. While these relations are intuitively appealing, at least to the author, they have not been rigorously established. The problem, of course, stems from the fact that the model proposed here is fundamentally nonstationary in nature due to the presence of the switch. On the other hand, the archival data dealing with human pilot dynamics, have been obtained using spectral measurement techniques which tacitly assume that the human is fundamentally stationary in his tracking behavior. Thus, one is presented with something of a dilemma in attempting to select parameters in a model like that of Fig. 1 to match archival data. It is sufficient to say that the analysis just described offers an approximate means of doing this. As will be seen, the nonstationary aspects of the model are mitigated by the fact that error rather than error rate control dominates, i.e., the parameter selection procedure to be described indicates $P_I \leq 0.25$ for all the tasks studied.

After the remnant scale factor $\rho = 0.38$ had been obtained on the basis of remnant data for pure gain dynamics, data fits for the remaining controlled-element dynamics and nonideal viewing condition were obtained in a straightforward manner and are discussed in Ref. 19. In these matches, the quality of the fit was determined by eye, i.e., no formal numerical criterion was employed.

Figures 2-7 show the model-generated and experimental describing functions and remnant spectral densities for controlled elements with dynamics of $Y_c = K$, K/s, K/s^2, $K/s(s-1)$, $K/s(s^2+1.414s+1)$, and K/s with 22 deg peripheral viewing. Data for the first three dynamics were taken from Ref. 2, the fourth and sixth dynamics from Ref. 20, and the fifth dynamics from Ref. 21. In all cases, the pilot's display was a CRT screen, and system error was presented by the displacement of a moving line from a fixed reference position. Control stick dynamics were negligible. In

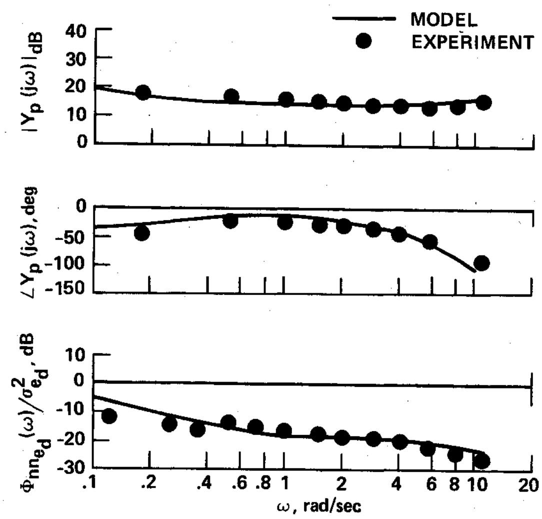

Fig. 3 Describing function and remnant comparison, K/s controlled-element dynamics.

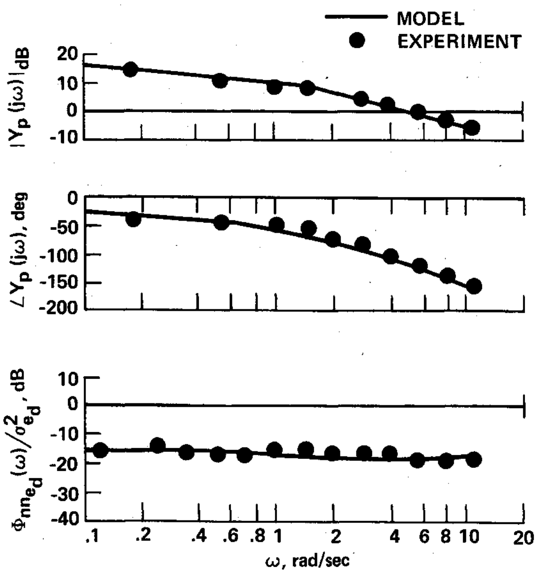

Fig. 2 Describing function and remnant comparison, K controlled-element dynamics.

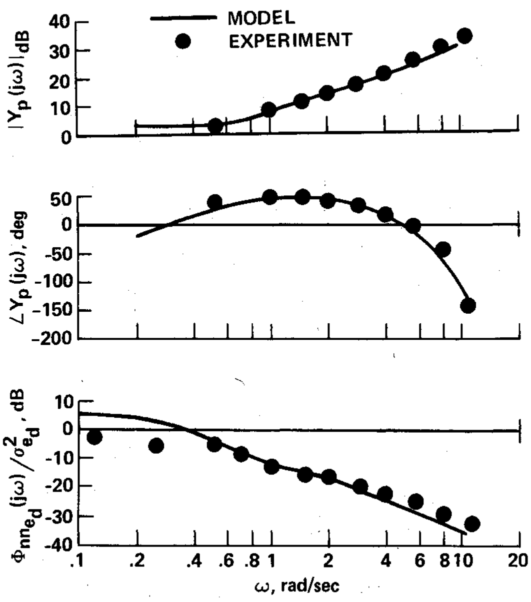

Fig. 4 Describing function and remnant comparison K/s^2 controlled-element dynamics.

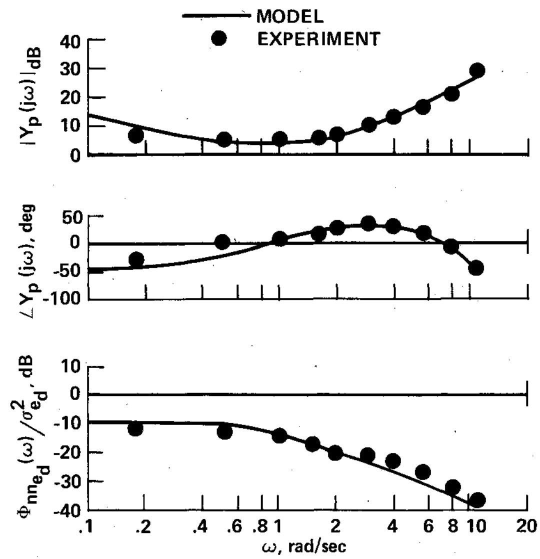

Fig. 5 Describing function and remnant comparison, $K/s(s-1)$ controlled-element dynamics.

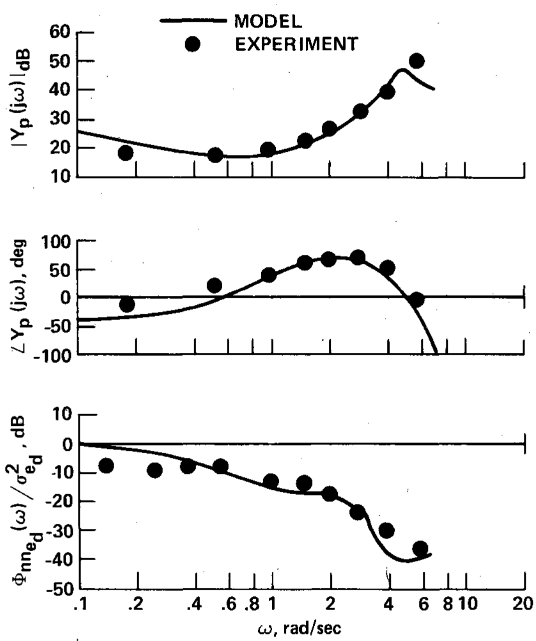

Fig. 6 Describing function and remnant comparison, $K/s(s^2+1.414s+1)$ controlled-element dynamics.

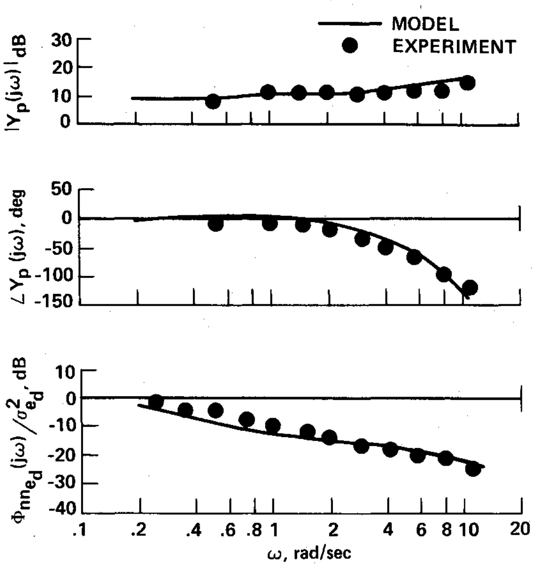

Fig. 7 Describing function and remnant comparison, K/s controlled-element dynamics, 22 deg peripheral viewing.

those cases where the data assumed remnant injected into error rate, and equivalent error-injected spectrum was calculated. Note that for remnant representation, the decibel is defined as 10 $\log_{10}(\cdot)$. Table 1 summarizes the model parameters used to obtain the figures using the approximation scheme just outlined. The dynamics of the first four controlled elements are identical to those used in Ref. 10, where an earlier form of the pilot model was used to match the data. In each case, the fits obtained here are superior to those of Ref. 10, and fewer model parameters need to be varied in order to obtain these fits (eight parameters in Ref. 10 as opposed to five here).

Discussion

Adapting to Vehicle Dynamics

$Y_c = K$ (Fig. 2)

The model and experimental describing function exhibits the first-order lag characteristics one would expect when pure gain dynamics are being controlled. Of particular interest is the model's ability to match the low-frequency phase lag apparent in the data. The earlier form of the model discussed in Ref. 10 did not provide a satisfactory match to this low-frequency phase data. The model and experimental injected remnant spectra are quite flat in the frequency range of interest. As mentioned previously, this experimental remnant was used to obtain the ρ value shown in Table 1.

$Y_c = K/s$ (Fig. 3)

Here the model and experimental describing functions exhibit the pure gain characteristics associated with rate dynamics. Again, note the model's ability to match the low-frequency phase lag (or phase "droop") in the data. The remnant match is particularly interesting in that the model is indicating a low-frequency rise in remnant power. In fact, rather than resembling the first-order process suggested by Levison et al.,[17] the remnant looks more like that offered by Pew[22]:

$$\Phi nn_{e_d}(\omega)/\sigma^2_{e_d} = 0.04\cdot(\omega)^{-0.8}$$

The ability of measured remnant spectra to exhibit shapes not amenable to description by a first-order process has been noted by other researchers in addition to Pew, e.g., Jex et al.[23] To the author's knowledge, however, this is the first time a model-generated remnant has exhibited these characteristics.

$Y_c = K/s^2$ (Fig. 4)

Here, a first-order lead is evident in the describing function data. Calculation of the model transfer function with the switch in the zero position demonstrated that the lead is attributable to the closed-loop characteristics of the inner feedback loops in the model, not to the error rate utilization. The model-generated remnant spectrum now appears more like a first-order process. Here, for the first time, significant switching activity is involved in the model, i.e., $P_l = 0.2$ as indicated in Table 1.

$Y_c = K/s(s-1)$ (Fig. 5)

The unstable dynamics again precipitate apparent lead equalization in the model. Again, however, this is due to inner loop activity, not error rate utilization. In Ref. 10, the model structure had to be altered to allow for actual, continuous error-lead equalization to match this data.

$Y_c = K/s(s^2 + 1.414s + 1)$ (Fig. 6)

These dynamics are interesting in that they resemble a K/s^3 plant in and beyond the region of crossover. Second-order apparent lead equalization is evident in model and data. The model exhibits more phase droop than the data, but, in general, the describing function fit is quite acceptable, particularly since Ref. 21 indicates that a substantial fraction of the pilot's output power was remnant related. It should be noted that the effective K/s^3 dynamics will probably induce pulsive or even impulsive control activity on the part of the pilot. Although no mention of such activity was made in Ref. 21, Jex and Allen[24] found that extremely pulsive control action accompanied "double-lead" equalization in a series of compensatory tracking tasks which they were studying. As mentioned previously, pulsive activity can be included in this model and is discussed in detail in Ref. 11. In terms of its effect on model-describing function and remnant, the pulsive activity associated with this task will quite likely lower the apparent damping ratio of the closed-loop neuromuscular mode roots. This would, in turn, improve the high-frequency remnant and describing function matches of Fig. 6.

Comments

As Table 1 indicates, the generation of the remnant power spectral densities and the various lags, leads, low-frequency phase droops, and changes in high-frequency phase lags evident in the overall model-describing function u_δ/e_d were obtained without changing the fundamental structure of the model or the values of the basic time delays (τ_0, τ_1), open-loop neuromuscular system parameters (ζ_n, ω_n, and K_1), and model output-injected remnant scale factor ρ. The pilot's adaptation to different controlled-element dynamics was accounted for by changes in the "internal model" of these dynamics, as reflected in changes in k, and in the parameters K_e, $K_{\dot{e}}$, K_2, P_1, and T_1, primarily associated with information processing in that portion of the model representing higher levels of the central nervous system.

Adapting to Displays of Varying Quality

The experimental describing function and remnant of Fig. 7 correspond to experimental conditions identical to those which yielded the data of Fig. 3 except that the display was located 22 deg off the pilot's foveal axis at all times. Comparing the describing functions (both model and experimental) for the peripheral as opposed to the foveal viewing, one finds an increase in high-frequency phase lags (or "effective" time delay), a decrease in low-frequency phase lags, a decrease in crossover frequency, and a concomitant increase in phase margin. Comparing the remnant (both model and experimental) for the two tasks reveals a significant increase in low-frequency remnant power for the peripheral viewing case. Comparing the entries in the second and last rows of Table 1 indicates that these changes in the model-generated describing function and remnant in going from foveal to peripheral are attributable primarily to reductions in the gains K_e and K_2 and an increase in the probability of the switch being in position 1, P_1. An analysis of each of these factors shows that the increased error rate tracking P_1 is responsible for both the increase in low-frequency remnant power and decrease in low-frequency phase lag. The decrease in K_2 accounts for 70% of the increase in high-frequency phase lag, the rest being attributable to the increase in P_1. Finally, the decrease in crossover frequency and increase in phase margin is due to the decrease in the gain K_e.

Fitting experimental data for this peripheral viewing experiment would be of little more than academic interest were it not for the fact that the changes in describing function and remnant just described have been shown to accompany other experimental studies involving degradation in display quality such as displays with "nonideal" quantized formats, etc.[23] Tactile displays can often be placed in this category. Recently, Schmid and Bekey[25] conducted tracking experiments involving an electrotactile display. One of their primary findings was that the particular electrotactile display which they utilized induced considerably larger high-frequency phase lags (or effective time delays) in the describing functions of the test subjects, as compared to those normally found in visual tracking with ideal display formats. Thus, the model parameter variations involved in matching data for the pair of tracking tasks involving foveal and peripheral viewing conditions may be useful in describing the manner in which the human adapts to any display degradation.

Conclusions

A model of the human pilot has been offered, which is an outgrowth of work reported in Refs. 9-11. Two features of the model distinguish it from other representations of the human pilot. First, proprioceptive information from the control stick or manipulator constitutes one of the major feedback paths in the model, providing feedback of vehicle output rate due to control activity. Implicit in this feedback loop is a model of the vehicle dynamics valid in and beyond the region of crossover. Second, error rate information is continuously derived and independently but intermittently controlled. An output-injected remnant model was offered and qualitatively justified on the basis of providing a measure of the effect of inaccuracies, such as time variations in the pilot's internal model of the controlled-element dynamics. By varying the values of only five parameters, the data from experimental tracking tasks involving five different controlled-element dynamics and one nonideal viewing condition were matched with model-generated describing functions and remnant power spectral densities. These model-generated results were obtained using a computational scheme which approximated the describing functions and remnant power spectral densities that would have been obtained if the model had been physically implemented and classical spectral techniques employed in measurement. The controlled-element dynamics varied in terms of control difficulty from the nondemanding K and K/s dynamics to the K/s $(s-1)$ and $K/s(s^2+1.414s+1)$ dynamics which approached the limits of manual control. It was indicated that the model characteristics, which resulted from matching the data for the peripheral viewing experiments, were qualitatively similar to measured pilot characteristics for a variety of tasks in which display quality was degraded.

In terms of utility, the model shows more potential in the area of data interpretation rather than in prediction. One such interpretative effort has been completed using an earlier form of the model[10] to provide a rationale for human operator pulsive control behavior.[11] Work is currently underway in extending the model to explain pursuit as well as compensatory tracking behavior.

References

[1] McRuer, D.T., Graham, D., Krendel, E., and Riesener W. Jr., "Human Pilot Dynamics in Compensatory Systems," Air Force Flight Dynamics Laboratory, AFFDL-TR-65-15, 1965.

[2] Kleinman, D.L., Baron, S., and Levison, W.H., "An Optimal Control Model of Human Response, Part I," *Automatica*, Vol. 6, 1970, pp. 357-369.

[3] Clement, W.F., McRuer, D.T., and Klein, R.G., "Systematic Manual Control Display Design," *Guidance and Control Displays*, AGARD CP-96, Oct. 1971, pp. 6-0 to 6-10.

[4] Hess, R.A., "Analytical Display Design for Flight Tasks Conducted Under Instrument Meteorological Conditions," *IEEE Transactions on Systems, Man and Cybernetics*, Vol. SMC-7, June 1977, pp. 453-462.

[5] Anderson, R.O., "A New Approach to the Specification and Evaluation of Flying Qualities," Air Force Flight Dynamics Laboratory, AFFDL-TR-69-120, 1970.

[6] Hess, R.A., "Prediction of Pilot Opinion Ratings Using an Optimal Pilot Model," *Human Factors*, Vol. 19, No. 5, 1977, pp. 459-475.

[7]Ringland, R.E., Stapleford, R.L., and Magdaleno, R.E., "Motion Effects on an IFR Hovering Task—Analytical Predictions and Experimental Results," NASA CR-1933, 1971.

[8]Levison, W.H. and Junker, A.M., "A Model for the Pilot's Use of Motion Cues in Roll-Axis Tracking Tasks," Aerospace Medical Research Laboratory, AMRL-TR-77-40, 1977.

[9]Smith, R.H., "A Theory for Handling Qualities with Applications to MIL-F-8785B," Air Force Flight Dynamics Laboratory, AFFDL-75-119, 1976.

[10]Hess, R.A., "A Dual-Loop Model of the Human Controller," *Journal of Guidance and Control,* Vol. 1, July-Aug. 1978, pp. 254-260.

[11]Hess, R.A., "A Rationale for Human Operator Pulsive Control Behavior," *Journal of Guidance and Control,* Vol. 2, May-June 1979, pp. 221-227.

[12]Kolers, R.A., *Aspects of Motion Perception,* Pergamon Press, New York, 1972, Chap. 3.

[13]McRuer, D.T., et al., "New Approaches to Human Pilot/Vehicle Dynamic Analysis," Air Force Flight Dynamics Laboratory, AFFDL-TR-67-150, 1968.

[14]Magdaleno, R.E. and McRuer, D.T., "Experimental Validation and Analytical Elaboration for Models of the Pilot's Neuromuscular Subsystem in Tracking Tasks," NASA CR-1757, 1971.

[15]Granit, R., *The Basis of Motor Control,* Academic Press, London and New York, 1970, Chap. VII.

[16]Kessel, C. and Wickens, C.D., "The Internal Model: A Study of the Relative Contribution of Proprioception and Visual Information to Failure Detection in Dynamic Systems," *Proceedings of the Fourteenth Annual Conference on Manual Control,* 1978, pp. 85-97.

[17]Levison, W.H., Baron, S., and Kleinman, D.L., "A Model for Human Controller Remnant," *IEEE Transactions on Man-Machine Systems,* Vol. MMS-10, Dec. 1969, pp. 101-108.

[18]Skelton, R.E. and Likins, P.L., "Techniques of Modeling and Model Error Compensation in Linear Regulator Problems," in *Control and Dynamic Systems,* edited by C.T. Leondes, Vol. 14, 1978, pp. 3-98.

[19]Hess, R.A., "A Structural Model of the Adaptive Human Pilot," AIAA Paper 79-1784, Aug. 1979.

[20]Levison, W.H., Elkind, J.I., and Ward, J.L., "Studies of Multivariable Manual Control Systems, A Model for Task Interference," NASA CR-1746, 1971.

[21]Levison, W.H., "The Effects of Display Gain and Signal Bandwidth on Human Controller Remnant," Aerospace Medical Research Laboratory, AMRL-TR-70-93, 1971.

[22]Pew, R.W., Duffendock, T.C., and Fensch, L.K., "Summary of Sine-Wave Tracking Studies," *Proceedings of the Second Annual Conference on Manual Control,* 1966, pp. 15-24.

[23]Jex, H.R., Allen, R.W., and Magdaleno, R.E., "Display Format Effects on Precision Tracking Performance, Describing Functions, and Remnant," Aerospace Medical Research Laboratory, AMRL-TR-71-63, 1971.

[24]Jex, H.R. and Allen, R.W., "Research on a New Human Dynamic Response Test Battery," *Proceedings of the Sixth Annual Conference on Manual Control,* 1970, pp. 743-777.

[25]Schmid, H.P. and Bekey, G.A., "Tactile Information Processing by Human Operators in Control Systems," *IEEE Transactions on Systems, Man, and Cybernetics,* Vol. SMC-8, Dec. 1978, pp. 860-866.